Adhesion-driven buckling of single-walled carbon nanotube bundles

Changhong Ke,[1,a] Meng Zheng,[1] In-Tae Bae,[2] and Guangwen Zhou[1]
[1]*Department of Mechanical Engineering, State University of New York at Binghamton, Binghamton, NY 13902-6000, USA*
[2]*Small Scale Systems Integration and Packaging Center, State University of New York at Binghamton, Binghamton, NY 13902-6000, USA*

(Received 1 February 2010; accepted 2 March 2010; published online 20 May 2010)

Buckling of a thin single-walled carbon nanotube (SWNT) bundle that is partially bound on another straight free-standing SWNT bundle is reported. The buckling of the SWNT bundle is purely due to the adhesion interaction between two SWNT bundles. The deformation curvature of the buckled SWNT bundle is experimentally measured by transmission electron microscopy, and is theoretically modeled by a continuum model based on nonlinear elastica theory. Our results reveal that the binding strength of the bundle interface and the bulk elastic modulus of the SWNT bundle can be associated by its buckling curvature. Our results show that the bulk elastic moduli of the tested SWNT bundles are significantly lower than the Young's modulus of individual SWNTs. The reported adhesion-driven nanotube buckling provides a potential new approach to quantify the elastic modulus and the binding strength of bundled nanotubes. © *2010 American Institute of Physics*. [doi:10.1063/1.3374469]

I. INTRODUCTION

Single-walled carbon nanotubes (SWNTs)[1] are a unique type of high aspect ratio nanostructure with extraordinary mechanical,[2,3] electrical,[4,5] and thermal properties,[6,7] which are currently being pursued for a variety of applications, including electronics,[8] sensors,[9] and composites.[10] SWNTs can undertake significant deformations, without apparent plasticity and catastrophic failure.[11,12] The excellent elastic behaviors of SWNTs and their high mechanical strength make them attractive materials for precision metrology[13] and flexible and stretchable device applications,[14] such as nanotube-based flexible transistors.[15–17] Recently, Huang and Rogers reported the buckling of well aligned individual SWNTs on prestretched polymer substrates.[18] From the waveform of the buckled nanotube on the substrate, the mechanical moduli of the nanotube, and the substrate materials can be determined based on continuum models.[18–20] In this paper, we report the buckling of a thin SWNT bundle on another partially bound free-standing straight SWNT bundle, as illustrated in Fig. 1(A). Unlike the buckling of SWNTs on polymer substrates, the buckling of the SWNT bundle presented here is due to the adhesion interactions among SWNTs on the binding interface of two bundles. Our results show that the bulk elastic modulus of bundled nanotubes and the binding strength between the nanotube bundles can be associated through the deformation curvature of the buckled SWNT bundle. Since as-grown SWNTs are more often in a bundled form than individual fibers due to the strong intertube van der Waals interactions, the information of the elastic modulus and binding interactions of bundled SWNTs will be very useful in the pursuit of their applications.

[a]Author to whom correspondence should be addressed. Electronic mail: cke@bingahtmon.edu. Tel.: 607-777-4782. FAX: 607-777-4620.

II. RESULTS AND DISCUSSION

The SWNTs employed in this study were originally grown on a Si wafer by chemical vapor deposition method.[21] A mechanical scratch approach[11] was employed to transfer as-grown SWNTs from the Si wafer to a transmission electron microscopy (TEM) copper grid (purchased from Ted Pella, Inc.) as thin free-standing bundles across the through-windows of the grid. A JEM 2100F high resolution TEM (HRTEM) was employed to inspect the SWNT bundles on the grid. Our HRTEM imaging reveals that the nanotubes in the bundle are parallel to one another and are held tightly presumably by van der Waals forces among them. It is noted that the obtained free-standing SWNT bundles on the TEM copper grids are consistently aligned parallel to the mechanical scratching direction.[11] For some of the SWNT bundles, as

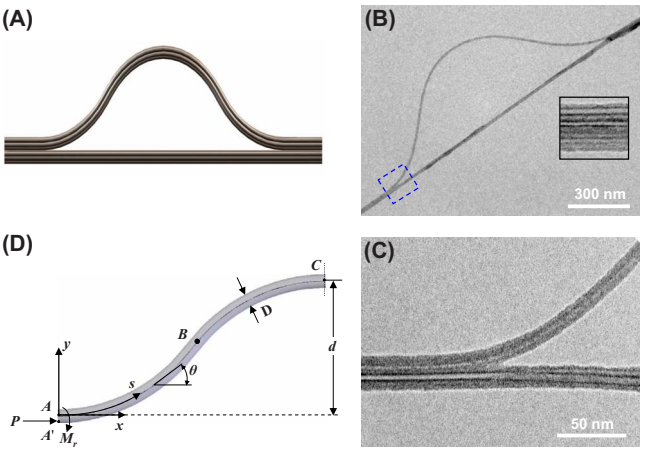

FIG. 1. (Color online) (A) Schematic of the adhesion-driven buckling of a SWNT bundle on another partially bound SWNT bundle; (B) TEM image of a buckled SWNT bundle that is partially bound on another free-standing straight SWNT bundle (the inset shows tubes in the buckled bundle); (C) magnified view of the selected area in (B); (D) schematic of the elastica model of one half of the buckled SWNT bundle.

exemplified by the TEM image shown in Fig. 1(B), part of the SWNT bundle are buckled and delaminated/separated from another partially bound straight bundle. Because both the buckled and straight bundles are free-standing structures, it is clear that the observed buckling of the SWNT bundle is purely due to the adhesion interactions between the SWNTs in both bundles. The buckling of the SWNT bundle is likely due to relative sliding between two originally bound SWNT bundles as a result of the fact that the strong axial force applied to the buckled bundle that was generated from the mechanical scratching process overcomes the interbundle binding force. Our image analysis shows that the shape of the buckled SWNT bundle is identical to that of the first buckling mode of a fixed-fixed column, which is completely symmetric with respect to its central line and the shape of the half buckled column is completely antisymmetric with respect to its inflection point. A magnified view of the deformation curvature of the buckled SWNT bundle shown in Fig. 1(B) around the separation line is shown in Fig. 1(C).

From the deformation curvature of the buckled SWNT bundle, we estimate the buckling force and the binding strength between these two SWNT bundles using a continuum model. Our TEM images clearly show that the deformation of the buckled SWNT bundle is in the large displacement regime. Therefore, we model the buckled SWNT bundle as an inextensible elastica rod.[22] This modeling assumption is consistent with the prior experimental observation that nanotubes could be repeatedly bent to large angles and strain without permanent distortion of the tube topography.[23] Due to the symmetric configuration, we only model one half of the buckled rod, which is illustrated in Fig. 1(D). In this model, the rod with lateral dimension D is buckled by a force P acting at point A', which is located at the left-bottom of the rod and interfacing with the straight bundle (not shown). The reaction moment at point A' is denoted as M_r. Point B is the inflexion point on the buckled rod. For simplification, we only consider the adhesion interaction between both bundles at their binding interfaces, while reasonably ignoring the van der Waals interaction between the buckled portion of the bundle and the fixed bundle. The deformation curvature of the rod is given by

$$EI\frac{\mathrm{d}^2\theta}{\mathrm{d}s^2} + P\sin(\theta) = 0, \tag{1}$$

where E and I are the Young's modulus and moment of inertial of the rod, respectively, s is the arc length along the deformed rod, and θ is the angle between the tangent of the rod at s and x-axis. The boundary conditions at points A, B, and C are $y_A=0$, $\theta_A=0$, $(\mathrm{d}\theta/\mathrm{d}s)|_B=0$, $y_c=d$, and $\theta_c=0$. In addition, it can be clearly seen that $\mathrm{d}\theta/\mathrm{d}s \geq 0$ for segment AB and $\mathrm{d}\theta/\mathrm{d}s \leq 0$ for segment BC, and $(\mathrm{d}\theta/\mathrm{d}s)|_A = -(\mathrm{d}\theta/\mathrm{d}s)|_C = (M_r - (PD/2)/EI)$. The buckling force P is given by $P=2M_r/(d+D)$. Following the approach reported in Ref. 22, we obtain

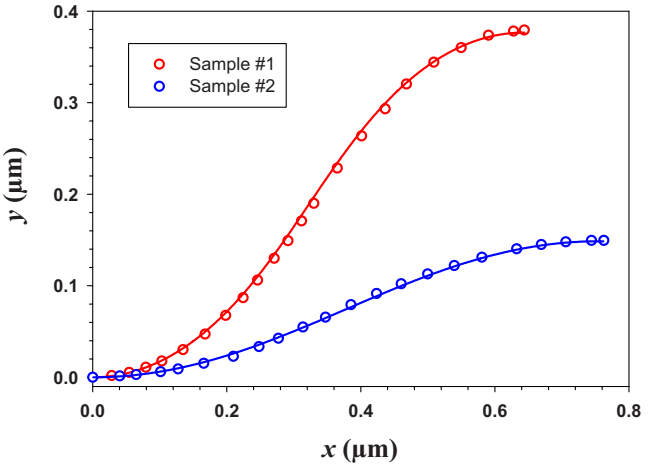

FIG. 2. (Color online) Deformation curvatures of two buckled SWNT bundles. The round circle represents the experimental data measured directly from the respective HRTEM images. The solid lines represent the respective theoretical predictions. The curves in red (light gray in print) are for the bundle shown in Fig. 1(B).

$$\frac{\mathrm{d}\theta}{\mathrm{d}s} = \pm\sqrt{\frac{\beta d}{d+D}\left[\frac{\beta d}{d+D}+\frac{4}{d}(\cos\theta - 1)\right]}, \tag{2}$$

where $\beta = M_r/EI$. Considering $\mathrm{d}x = \mathrm{d}s\cos\theta$ and $\mathrm{d}y = \mathrm{d}s\sin\theta$, the deformation curvature of the buckled rod in the (x,y) coordinate system can be determined. The total length of the buckled rod, L, is four times of the curve length of segment AB and is given by

$$L = \int_0^{\theta_B} \frac{4\mathrm{d}\theta}{\sqrt{\frac{\beta d}{d+D}\left[\frac{\beta d}{d+D}+\frac{4}{d}(\cos\theta - 1)\right]}}, \tag{3}$$

where θ_B is the slope of the rod at the inflexion point B and is measured directly from the captured TEM images.

Using the above theoretical model, we analyze two selected buckled SWNT bundle samples, including the one shown in Fig. 1(B). Deformation curvatures of both samples are measured directly from the respective TEM images. The comparison between experimental measurements and theoretical predictions for half of the buckled bundle for both samples are presented in Fig. 2. It is clear that theoretical predictions are in good agreement with experimental measurements with β as the only fitting parameter. The estimated reaction moment, buckling force, and SWNT bundle length for both samples are presented in Table I. For fixed-fixed columns, the critical load for buckling is given by $P_{cr} = (4\pi^2/L^2)EI$. For our examined SWNT bundles, the calculated critical loads, normalized by EI, are 16.62 $\mu\mathrm{m}^{-2}$ for sample no. 1 and 16.35 $\mu\mathrm{m}^{-2}$ for sample no. 2, respectively. Both values are slightly lower than the buckling forces estimated using our elastica model.

The buckled SWNT bundle can be considered to be delaminated from the straight bundle due to the balance between the bending moment at the separation line and the reaction moment due to the adhesion interactions between two bundles. The binding energy per unit length (along the axial direction of the bundles) between the buckled and

TABLE I. Two buckled SWNT bundles and the estimated reaction moment M_r, buckling force P, and binding energy between the buckled and the straight SWNT bundles γ. Sample no. 1 is shown in Fig. 1(B).

Sample	D (nm)	d (nm)	θ_B (°)	L (μm)	$M_r/(EI)$ (μm^{-1})	$P/(EI)$ (μm^{-2})	γ/E (pm) Semicircle	γ/E (pm) Rectangle
No. 1	13.4	379	47.4	1.54	3.52	17.97	1.246	0.821
No. 2	24.4	150	17.5	1.55	1.44	16.57	1.256	0.827

straight bundles is given by[24] $G=(1/2)(M_r^2/EI)$. Due to the overlapping effect, the exact tube assembly configuration in the SWNT bundles cannot be readily measured by HRTEM. Here we consider two possible cross-section shapes for the buckled bundle, including rectangle and semicircle as illustrated in Fig. 3(A). The per-unit-area binding energy between two SWNT bundles, γ, is given by

$$\gamma=\frac{G}{b}=\frac{\beta^2 I}{2b}E, \tag{4}$$

in which b is the contact length. The binding energy γ, normalized by E, are calculated for both samples and presented in Table I. Assuming that E is independent on the nanotube assembly configuration in the bundle, our results show that the estimated γ is highly dependent on the cross-section shape of the bundle. It is interesting to note that the estimated γ for both samples are quite close to each other, implying that they possess similar tube assembly configuration.

Prior studies show that the Young's modulus of the SWNT bundle is dependent on the diameter of the tubes in the bundle and decreases with the increase of the tube diameter.[25] This is due to the fact that the intertube van der waals interaction is significantly weaker than the axial strength of individual tubes which is ascribed to the covalent bonding and can be accurately predicted using interatomic potential-based theoretical models.[26–28] The bulk elastic modulus of SWNT bundles could be significantly lower than that of individual SWNTs (~1 TPa), and may even approach the shear modulus of individual SWNTs (~1–10 GPa).[29] From Eq. (4), we can estimate the bulk elastic modulus of the SWNT bundles using the theoretically predicted γ based on the van der Waals interactions between two bundles, or vice versa.

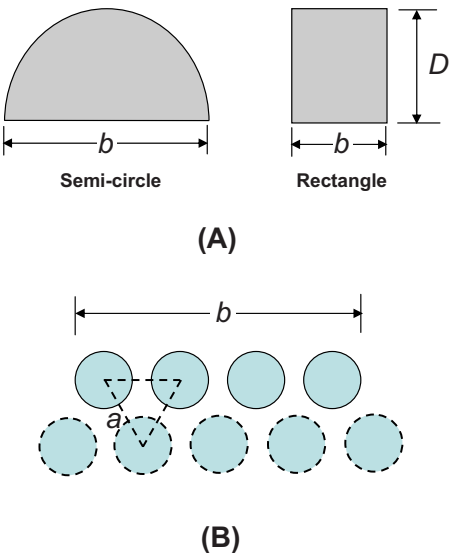

FIG. 3. (Color online) (A) Two possible cross-section shapes of the buckled SWNT bundle; (B) schematic of the adhesion interface between the buckled and the straight SWNT bundles. The solid circles represent the interface SWNTs in the buckled SWNT bundle. The dotted circles represent the interface SWNTs in the straight SWNT bundle.

The average diameter of the tubes in our samples is measured to be $D_{CNT}\approx 1.5$ nm based on TEM images, which is close to that of (11, 11) tubes. We reasonably assume that the tubes in the bundle remain circular[30] and form an orderly hexagonal structure,[31] and consider the tube arrangement on the bundle interface as illustrated in Fig. 3(B). The adhesion energy on the bundle interface due to the van der Waals interactions between neighboring SWNTs can be theoretically predicted using a continuum model based on Lennard–Jones potential.[32] The equilibrium lattice constant for the bundled tubes, which corresponds to the minimum total van der Waals energy, is given by $a=D_{CNT}+0.313$ nm.[33] The corresponding adhesion energy per unit area on the bundle interface is approximated by,[33] $\gamma^{Theo}\approx 3\pi n_\sigma^2/4r^3 a[-AI_A+(21B/32r^6)I_B]$, in which $n_\sigma=38/\text{nm}^2$ is the graphene surface density, I_A and I_B are two double integrals and functions of a/r, and $A=15.2$ eV·Å^6 and $B=24.1$ keV·Å^{12}. Using the above parameters, the adhesion energy is calculated as $\gamma^{Theo}=0.175$ J/m^2. The estimated bulk elastic moduli of the SWNT bundles are 140 GPa (for rectangular cross-section) and 212 GPa (for semicircular cross-section). Both the estimated values are significantly lower than the Young's modulus of individual SWNT fibers, while significantly higher than their shear modulus. As mentioned earlier, the observed low Young's modulus of the tested SWNT bundles is likely due to the fact that the van der Waals interaction-based intertube binding strength is significantly weaker than the covalent bond-based axial strength of individual SWNTs. Possible defects in SWNT structures, such as Stone–Wales transformation[34] that may either pre-exist or be generated during the nanotube deformation process, may also significantly lower the elastic strength of SWNT bundles.[35,36] Similarly, provided that the bulk elastic modulus of the SWNT bundle is known, the binding energy between two SWNT bundles can be readily determined.

III. CONCLUSION

In this paper, we present a study of the adhesion-driven buckling of thin SWNT bundles. Deformation curvatures of the buckled SWNT bundles were experimentally measured

by TEM and theoretically modeled by a continuum model based on nonlinear elastica theory. Our results reveal that the binding strength of the bundle interface and the bulk elastic modulus of the nanotube bundle can be correlated through the deformation curvature of the buckled nanotube bundle. The bulk elastic moduli of the tested SWNT bundles are estimated for two possible tube assembly configurations, and are found to be significantly lower than the Young's modulus of individual SWNTs. Our results show that the adhesion-driven nanotube buckling as presented in this paper provides a potential new approach to quantify the elastic strength and the binding interactions of bundled nanotubes.

ACKNOWLEDGMENTS

This work was supported by the State University of New York at Binghamton and was partially supported by American Chemical Society-Petroleum Research Fund. The TEM imaging work was performed using the facilities in the Analytical and Diagnostics Laboratory at Binghamton University's Small Scale Systems Integration and Packaging Center S3IP.

[1]M. S. Dresselhaus, G. Dresselaus, and P. Avouris, *Carbon Nanotubes* (Springer, Berlin, 2001).
[2]D. Qian, G. J. Wagner, W. K. Liu, M. F. Yu, and R. S. Ruoff, Appl. Mech. Rev. **55**, 495 (2002).
[3]B. Liu, H. Jiang, H. T. Johnson, and Y. Huang, J. Mech. Phys. Solids **52**, 1 (2004).
[4]P. Avouris, J. Appenzeller, R. Martel, and S. J. Wind, Proc. IEEE **91**, 1772 (2003).
[5]P. L. McEuen, M. S. Fuhrer, and H. K. Park, IEEE Trans. NanoTechnol. **1**, 78 (2002).
[6]H. Jiang, B. Liu, Y. Huang, and K. C. Hwang, J. Eng. Mater. Technol. **126**, 265 (2004).
[7]J. Hone, M. C. Llaguno, M. J. Biercuk, A. T. Johnson, B. Batlogg, Z. Benes, and J. E. Fischer, Appl. Phys. A: Mater. Sci. Process. **74**, 339 (2002).
[8]H. G. Craighead, Science **290**, 1532 (2000).
[9]B. Mahar, C. Laslau, R. Yip, and Y. Sun, IEEE Sens. J. **7**, 266 (2007).
[10]J. N. Coleman, U. Khan, and Y. K. Gun'ko, Adv. Mater. **18**, 689 (2006).
[11]C. Ke, M. Zheng, G. Zhou, W. Cui, N. Pugno, and R. N. Miles, Small **6**, 438 (2010).
[12]T. W. Tombler, C. W. Zhou, L. Alexseyev, J. Kong, H. J. Dai, L. Lei, C. S. Jayanthi, M. J. Tang, and S. Y. Wu, Nature (London) **405**, 769 (2000).
[13]C. M. Stafford, C. Harrison, K. L. Beers, A. Karim, E. J. Amis, M. R. Vanlandingham, H. C. Kim, W. Volksen, R. D. Miller, and E. E. Simonyi, Nature Mater. **3**, 545 (2004).
[14]Q. Cao and J. A. Rogers, Adv. Mater. **21**, 29 (2009).
[15]T. Takenobu, T. Takahashi, T. Kanbara, K. Tsukagoshi, Y. Aoyagi, and Y. Iwasa, Appl. Phys. Lett. **88**, 033511 (2006).
[16]Q. Cao, Z. T. Zhu, M. G. Lemaitre, M. G. Xia, M. Shim, and J. A. Rogers, Appl. Phys. Lett. **88**, 113511 (2006).
[17]E. Artukovic, M. Kaempgen, D. S. Hecht, S. Roth, and G. Grüner, Nano Lett. **5**, 757–760 (2005).
[18]D. Y. Khang, J. L. Xiao, C. Kocabas, S. MacLaren, T. Banks, H. Q. Jiang, Y. Y. G. Huang, and J. A. Rogers, Nano Lett. **8**, 124 (2008).
[19]J. Xiao, H. Jiang, D. Y. Khang, J. Wu, Y. Huang, and J. A. Rogers, J. Appl. Phys. **104**, 033543 (2008).
[20]D. Y. Khang, J. A. Rogers, and H. H. Lee, Adv. Funct. Mater. **19**, 1526 (2009).
[21]W. Z. Li, S. S. Xie, L. X. Qian, B. H. Chang, B. S. Zou, W. Y. Zhou, R. A. Zhao, and G. Wang, Science **274**, 1701 (1996).
[22]Y. Mikata, Acta Mech. **190**, 133 (2007).
[23]M. R. Falvo, G. J. Clary, R. M. Taylor, V. Chi, F. P. Brooks, S. Washburn, and R. Superfine, Nature (London) **389**, 582 (1997).
[24]O. A. Goussev, P. Richner, and U. W. Suter, J. Adhes. **69**, 1 (1999).
[25]J. P. Lu, Phys. Rev. Lett. **79**, 1297 (1997).
[26]P. Zhang, H. Jiang, Y. Huang, P. H. Geubelle, and K. C. Hwang, J. Mech. Phys. Solids **52**, 977 (2004).
[27]P. Zhang, Y. Huang, P. H. Geubelle, P. A. Klein, and K. C. Hwang, Int. J. Solids Struct. **39**, 3893 (2002).
[28]J. Wu, K. C. Hwang, and Y. Huang, J. Mech. Phys. Solids **56**, 279 (2008).
[29]A. Kis, G. Csanyi, J. P. Salvetat, T. N. Lee, E. Couteau, A. J. Kulik, W. Benoit, J. Brugger, and L. Forro, Nature Mater. **3**, 153 (2004).
[30]T. Tang, A. Jagota, and C. Y. Hui, J. Appl. Phys. **97**, 074304 (2005).
[31]A. Thess, R. Lee, P. Nikolaev, H. J. Dai, P. Petit, J. Robert, C. H. Xu, Y. H. Lee, S. G. Kim, A. G. Rinzler, D. T. Colbert, G. E. Scuseria, D. Tomanek, J. E. Fischer, and R. E. Smalley, Science **273**, 483 (1996).
[32]J. E. Lennard-Jones, Proc. R. Soc. London Ser. A **129**, 598 (1930).
[33]L. A. Girifalco, M. Hodak, and R. S. Lee, Phys. Rev. B **62**, 13104 (2000).
[34]G. G. Samsonidze, G. G. Samsonidze, and B. I. Yakobson, Comput. Mater. Sci. **23**, 62 (2002).
[35]H. Jiang, X. Q. Feng, Y. Huang, K. C. Hwang, and P. D. Wu, Comput. Methods Appl. Mech. Eng. **193**, 3419 (2004).
[36]K. I. Tserpes and P. Papanikos, Compos. Struct. **79**, 581 (2007).